

Field Deployable Mirror Soiling Detection Based on Polarimetric Imaging

Md Zubair Ebne Rafique¹[\[https://orcid.org/0009-0008-7507-2179\]](https://orcid.org/0009-0008-7507-2179), Hossain Mansur Resalat Faruque¹[\[https://orcid.org/0000-0001-5710-2145\]](https://orcid.org/0000-0001-5710-2145), Ahmed Hassan¹[\[https://orcid.org/0000-0003-1334-7161\]](https://orcid.org/0000-0003-1334-7161), Mo Tian¹[\[https://orcid.org/0009-0007-4785-431X\]](https://orcid.org/0009-0007-4785-431X), Nabasindhu Das¹[\[https://orcid.org/0009-0006-1542-1491\]](https://orcid.org/0009-0006-1542-1491), and Yu Yao¹[\[https://orcid.org/0000-0003-4892-052X\]](https://orcid.org/0000-0003-4892-052X)

¹ Electrical, Computer and Energy Engineering, Arizona State University. Tempe, AZ

Abstract. Heliostat mirror soiling is one of the significant factors for reduced optical efficiency of Concentrated Solar Power (CSP) fields. However, it remains challenging to determine the mirror soiling patterns across the large area of the CSP field. Here we propose a fast and field deployable inspection method to measure the heliostat mirror soiling levels based on polarization images in regular daylight settings without additional light sources. Under sunny and clear sky conditions, we have demonstrated accurate measurement of reflection efficiency (error ~1%) for mirrors with different soiling levels.

Keywords: Heliostat, Mirror Soiling Detection, Polarimetric Imaging, Reflection Efficiency

1. Introduction

Heliostat mirrors are used in concentrated solar power (CSP) plants to redirect and focus sunlight on receiver tubes to produce electricity. However, these mirrors can become soiled with small particles due to wind, dust storms, and many other natural environmental effects. Mirror soiling can lead to a significant reduction in the optical reflection efficiency (below 90%) of heliostats and can reduce the overall efficiency of the CSP plant. Therefore, sequential cleaning is required to maintain the maximum reflectivity of the heliostat mirrors in concentrated solar power plants to maintain the maximum efficiency of the whole plant. Currently, the soiling levels of the mirrors are usually determined by manual measurement using handheld reflectometers [1][2], which is slow and only covers a very small portion of the mirror surface. Furthermore, as they can only provide point measurements, the reflection from different parts of the mirror surface can be different. Thus, it is highly desirable to achieve large area measurements of the whole mirror surface to obtain the soiling condition across the heliostats rather than single point measurements. Furthermore, the heliostat mirror cleaning cost is ~25% of the CSP plant's total operation and maintenance cost [3]. Therefore, a fast and field-deployable method for detecting the soiling levels of heliostat mirrors is highly beneficial for planning CSP field collector cleaning to maintain low optical loss with minimal cleaning cost. Meanwhile, it can also facilitate the study of mirror soiling patterns in CSP fields. Here we show that polarization images of heliostat mirrors, esp. the degree of linear polarization (DoLP) images, can be used under sunny and clear sky conditions to measure the mirror soiling levels across the mirror facets in a single shot. We performed outdoor tests and determined mirror soiling levels up to reflection efficiencies of 98% with high accuracy (measurement error <1%), which is deemed challenging with conventional intensity imaging-based methods [4]–[6]. We also

show that the polarization imaging method can be deployed in CSP collector fields for in-situ characterization of the heliostat mirror soiling levels with high throughput and low labor cost.

2. Measurement, Simulation, and Analysis

2.1 Polarimetric Imaging of Mirror Soiling

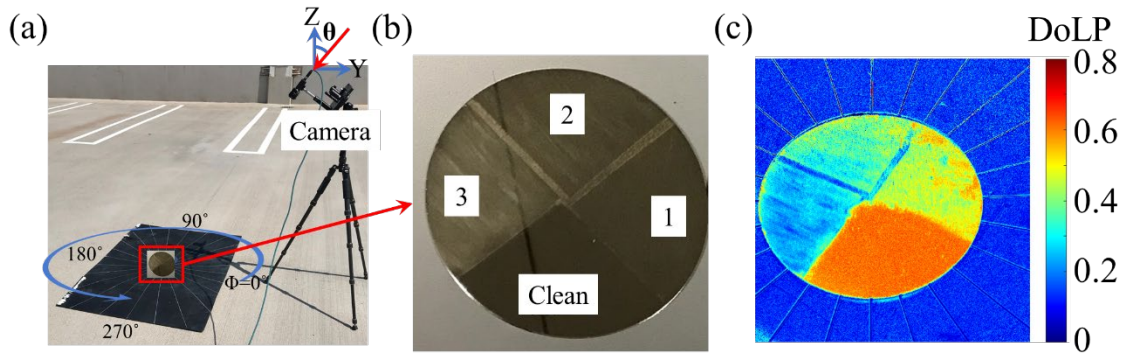


Figure 1. (a) Outdoor measurement setup with a polarization-sensitive camera and mirror sample. (b) Soiled mirror sample with different soiling levels in each quadrant. The soil sample is collected from the riverbank of Tempe town lake. The number sequence on represents increasing soiling concentration for each section resulting in 94.3%, 92.7% and 82.1% reflection efficiency consecutively relative to the clean section. The particle size distribution is shown in Figure 2b. (d) Processed DoLP image of the soiled mirror sample.

We performed polarization imaging of a soiled mirror with a polarization-sensitive camera (Lucid Vision Inc.). The camera consists of Sony's image sensor with four different polarizers (grating structures aligned at 0°, 90°, 45°, and 135°) on top of four neighboring image pixels. Intensity captured by these pixels can be interpreted to obtain the Stokes parameters (Q and U [7], [8]) of the incoming light, which can provide us with its linear polarization information. Figure 1a shows the setup we used for the outdoor measurement under a clear sky (cloud coverage <20%) on a sunny day. The polarization camera was mounted on a tripod to take pictures of the soiled mirror from different azimuth (Φ) and zenith (θ) angles. We used a granulated black cardboard indicating different azimuth angles. We prepared a soiled mirror with the small sand/dust particles collected from a nearby riverbank (Tempe Town Lake) for this demonstration. The prepared soiled mirror, Figure 1b, has four different regions with different soiling levels. The number sequence in Figure 1b indicates an increasing soiling level for sections 1, 2, 3, corresponding to relative reflection efficiencies (normalized by the reflection of the clean section) of 94.3%, 92.7%, and 82.1%, respectively.

By changing the azimuth (Φ) and zenith (θ) angle of the imaging setup, we can take a picture of any portion of the sky through the mirror. The tiny particles on the soiled mirror surface can scatter the incoming light. So, the images of the sky taken through the soiled mirror will contain modified polarization information because the camera image sensor collects both the reflected skylight and the scattered sunlight. Skylight is partially polarized and can be predicted reasonably well with the Mie theory [9]. The degree of linear polarization (DoLP) of the incident partially polarized skylight will decrease after being scattered by the particles. Therefore, mirrors with high soiling levels exhibit a large decrease of DoLP in the image compared to cleaner mirrors with lower soiling levels. More detailed discussions are presented in the next section. In the outdoor measurements, we took the

image of the sky from the mirror with the polarimetric imaging sensor to obtain the corresponding mapping of DoLP across the mirror surface, i.e., the DoLP image shown in Figure 1c. Here, one can clearly see the difference in DoLP in different soiled sections of the mirror. The maximum DoLP is observed in the clean part, and it gradually decreases with increasing soiling levels, as discussed before. In the following sections, we establish a relationship between the observed DoLP and the soiling levels (corresponding to different relative reflection coefficients) of the mirrors by combining outdoor measurements and a mathematical model and eventually predict the soiling level from this relationship for mirrors with unknown soiling levels.

2.2 Mathematical Model

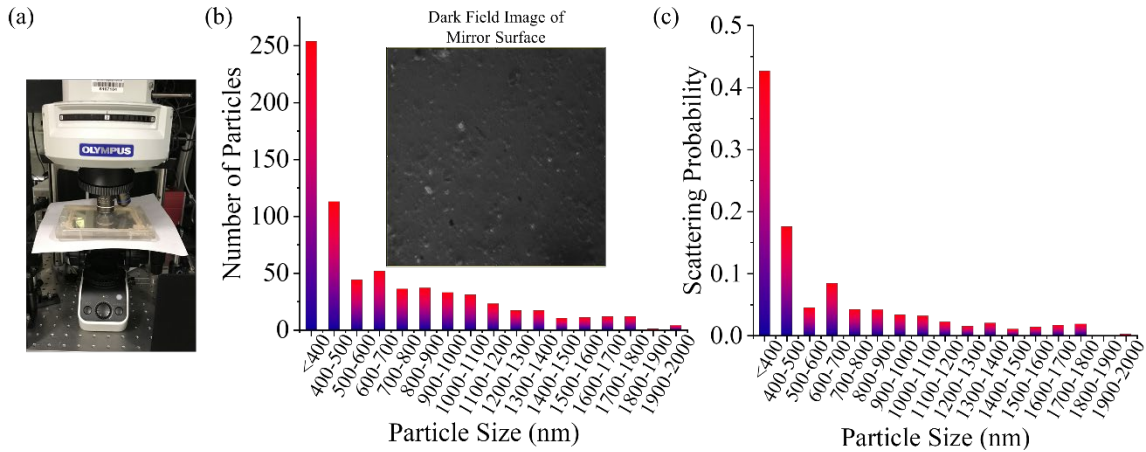


Figure 2. (a) Mirror soiling particle imaging system. (b) The number of particles vs. particle size (nm). Inset showing the dark field image of the mirror surface. (c) Scattering probability for different particle sizes.

To understand the light scattering from the soiled mirror, we studied the mirror surface utilizing dark-field imaging with a microscope, illustrated in Figure 2a. The dark field images, Figure 2b inset, show small particles on the mirror surface. The images were processed using a Matlab Image processor to identify different particles and determine their sizes (diameter). We obtained the particle size distribution on the mirror from this image analysis, illustrated in Figure 2b. These particles' scattering probability is calculated using the well-established Mie scattering theory [9]. The wavelength of light considered here is 530nm, the same as our polarization-sensitive camera's working wavelength. The particle index is 1.57 (sand), and the mirror glass is 1.52. The attenuation coefficients for each particle size are calculated considering the particle size, number density (m^{-2}) for each size, and the scattering and absorption cross-sections using the Mie scattering theory [10]. Furthermore, considering both the attenuation coefficient (U_t) and the number (N_D) of each particle size, one can calculate the scattering probability (P_i) of each of these particles, shown in Figure 2c.

If we put a soiled mirror lying on the ground on a sunny day, the unpolarized sunlight will be scattered by the small particles, and the partially polarized skylight will be reflected from the mirror surface, as illustrated in Figure 3a. The final polarization pattern seen from the soiled mirror is a combination of these two effects. Sunlight reflection, which produces overexposed images, and the skylight scattering by the particles are ignored as they produce fewer effects in the overall polarization map but come with a very large computational drag.

To simulate the sunlight scattering event and obtain the polarization pattern for sunlight scattering from the particles on the mirror, we have considered the coordinate system illustrated in Figure 3b. The XY plane is the mirror surface containing the particles, and Z-axis is the surface normal to the mirror. Incident light coming at a zenith angle, θ_i and azimuth angle, ϕ_i ; gets scattered, and the camera (at zenith angle, θ_D and azimuth angle ϕ_D) collects the scattered light. To account for the reflected scattered light, an image of the incident light source is considered at the zenith angle, θ_i^M and azimuth angle, ϕ_i .

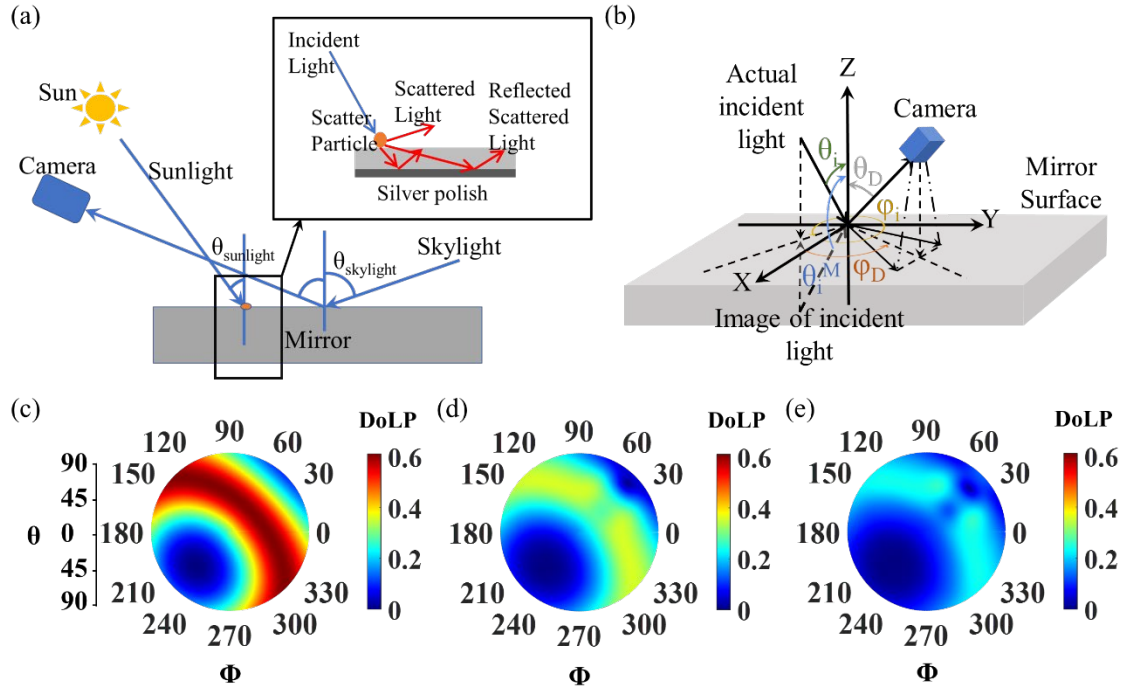


Figure 3. (a) Schematic illustration of mathematical model description. (b) The coordinate system for the Mie scattering simulation of sunlight. XY plane is on the mirror surface. (c-e) DoLP map seen from the mirror considering both skylight reflection and sunlight scattering. For mirror with (c) 100% reflection (fully clean mirror). (d) 90% reflection (e) 80% reflection. Simulation is done considering a clear sunny day on 03/01/2022 at 3:18pm. Location Arizona State University Church parking lot roof (33.419258°, -111.929590°).

The total polarization pattern is obtained by weighted summation (considering scattering probability, Figure 2c) of the polarization patterns of each particle in the particle size distribution. So, the overall stokes parameter for sunlight scattering is [11],

$$S_{Sun_Scat}(\theta, \phi) = \sum_{p=1}^N P_p \left[\left[R(\psi) \left\{ M^p(\alpha) \left(R(\psi) S_{Sun}(\theta_i, \phi_i) \right) \right\} \right] + \left[R(\psi) \left\{ M^p(\alpha) \left(R(\psi) S_{Sun}(\theta_i^M, \phi_i) \right) \right\} \right] \right] \quad (1)$$

Here, $S_{Sun_Scat}(\theta, \phi)$ is the stokes parameter after sunlight scattering, P_p is the scattering probability for each size of particles, p is particle size counter, S_{Sun} is the stokes parameter containing the polarization information of the incident light, in this case, sunlight. The scattering angle, α , is calculated as follows [9], $\cos\alpha = \sin\theta_i \sin\theta_D \cos(\phi_i - \phi_D) + \cos\theta_i \cos\theta_D$. The scattering matrix, $M^p(\alpha)$, works as a muller matrix that describes the change in the

polarization state of light after scattering from a particular particle. It is dependent on the properties of the particle, i.e., size of the particle, index of particle, and also the scattering angle. As it is different for each particle, so we indicate it with p notation. For a spherical particle, it is defined as below [9],

$$M^p(\alpha) = \begin{bmatrix} M_{11}(\alpha) & M_{12}(\alpha) & 0 & 0 \\ M_{21}(\alpha) & M_{11}(\alpha) & 0 & 0 \\ 0 & 0 & M_{33}(\alpha) & M_{34}(\alpha) \\ 0 & 0 & -M_{34}(\alpha) & M_{33}(\alpha) \end{bmatrix} \quad (2)$$

Here, $M_{11}=M_{22} = \frac{1}{2} (|m_1|^2 + |m_2|^2)$, $M_{12}=M_{21} = \frac{1}{2} (|m_2|^2 - |m_1|^2)$, $M_{33}=M_{44} = \frac{1}{2} (m_1^* m_2 + m_1 m_2^*)$, $M_{34}=-M_{43} = i \frac{1}{2} (m_1^* m_2 - m_1 m_2^*)$. m_1 and m_2 are the scattering functions representing the far-field solution of maxwell's equations. They were obtained using the Mie theory [10]. Moreover, $R(\psi)$ is the rotation matrix [9], used to rotate the incoming light polarization fields into the scattering plane ($R(\psi_1)$) and out of the scattering plane ($R(\psi_2)$), and ψ is the rotation angle.

In this model, we also consider that the skylight reflects from the mirror surface, as shown in Figure 3a, and the camera captures the reflected skylight. The skylight polarization map is obtained from the Rayleigh scattering theory [9]. Sunlight is scattered by Rayleigh scatterers, and it forms a partially polarized skylight, clearly described in [11]. We assume that the skylight reflected off the mirror does not change the polarization of the skylight.

The overall effect of sunlight scattering and skylight reflection is calculated using the following equation [11],

$$S_T = S_{Sun_Scat} R_{Sun} A_P + S_{Sky} R_{Sky} A_{NP} \quad (3)$$

Here, A_P is the percentage of the area on the mirror covered by particles and A_{NP} is the percentage of the area on the mirror not covered by particles. A_P and A_{NP} are calculated by considering the number of particle densities (m^{-2}), the area of the particles (utilizing the size and considering it as a circle), and the area of the image. R_{Sun} is the percentage of sunlight not converted to skylight and R_{Sky} is the percentage of sunlight converted to the skylight. $R_{Sun} : R_{Sky}$ ratio depends on different conditions such as weather, aerosol concentration in a certain area etc. For a bright sunny day, this ratio is considered to be $R_{Sun} : R_{Sky} = 70 : 30$. Stokes parameters are usually written as a column vector as follows [7], [8], $S = [I \ Q \ U \ V]$. Where I is the total intensity of light, Q is the difference between the linear horizontal (0°) and linear vertical (90°) polarization component of light, U is the difference between the linear $+45^\circ$ and linear -45° polarization component of light, and V represents the difference between the right circular and left circular polarization component of light. The degree of linear polarization of light is calculated as,

$$DoLP = \frac{\sqrt{Q^2 + U^2}}{I} \quad (4)$$

Figure 3c-e shows the polarization mapping seen through the mirror for different levels of soiling on the mirror. We can see from Figure 3(c-e) that the polarization pattern is non-uniform. These plots of the polarization map can help us determine where to look for

maximum contrast. So, we try to position our camera in such a way so that we point to some location where the DoLP is relatively uniform and the DoLP value is large. This can help us obtain maximum contrast for different soiling levels and remove any ambiguity in measurement, i.e., increase measurement reliability.

2.3 Mirror Soiling Prediction Methodology

To demonstrate the capability to predict soiling, we measured the DoLP of three more samples using our measurement setup illustrated in Figure 1a. The samples were made from the same dust collected from the local riverbank (Tempe Town Lake) and had four different parts in each mirror same as the previous sample. So, it is safe to say that the particle size distribution and scattering probability of the particles on these samples are also the same as presented in Figure 2b and c. The soiling levels of the samples were unknown during the measurement. The measurement was done on a building rooftop under clear sky (no clouds), and the looking direction (Φ , θ) was at the maximum DoLP in a uniform region of the polarization mapping obtained by the model (around $\Phi=330^\circ$ and $\theta=65^\circ$, in Figure 3c).

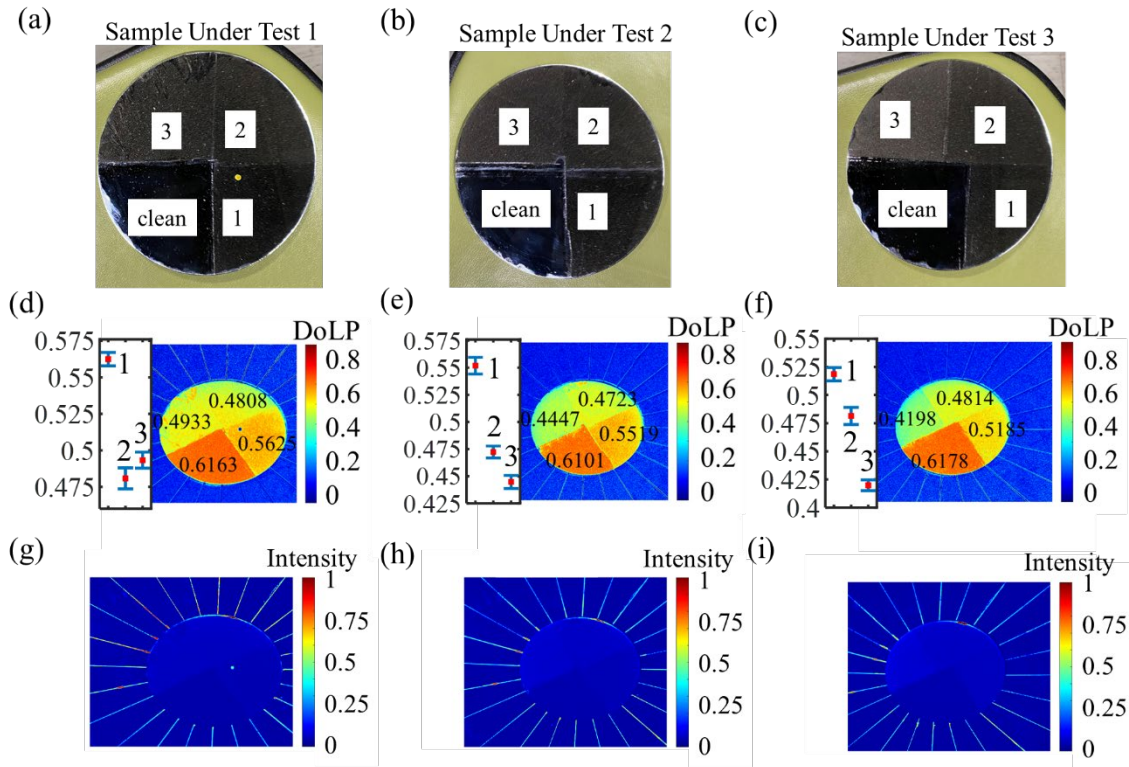


Figure 4. (a-c) Soiled mirror samples with unknown soiling levels in each quadrant. (d-f) DoLP image of the mirror samples. The median value of the DoLP is written on top of each section. The DoLP range in each section is shown on the side of each image. (g-i) Intensity image of the samples. Measurement is done on a clear sunny day (03/01/2022) at 3:18pm. Location Arizona State University Church parking lot roof (33.419258° , -111.929590°). Camera location azimuth, $\Phi=330^\circ$ and zenith, $\theta=65^\circ$.

The sample images (samples 1, 2 and 3), processed DoLP image, and the intensity images from the measurement are shown in Figure 4. The DoLP images of the samples show a decrease in DoLP values with the increase in soiling level, similar to the earlier demonstration in Figure 1c. On the other hand, the intensity images, Figure 4g-i, show very small changes for different soiling levels. As this is a large area measurement and not a

point measurement, we have more than one value of DoLP in each section (quadrature) of the samples in each image. The DoLP value range of each section of each sample is presented on the side of each DoLP image in Figure 4d-f. The median DoLP value of each section is written on top of the corresponding section. Uniform DoLP images suggest the corresponding regions have similar soiling levels, while variations in DoLP images suggest non-uniform soiling patterns.

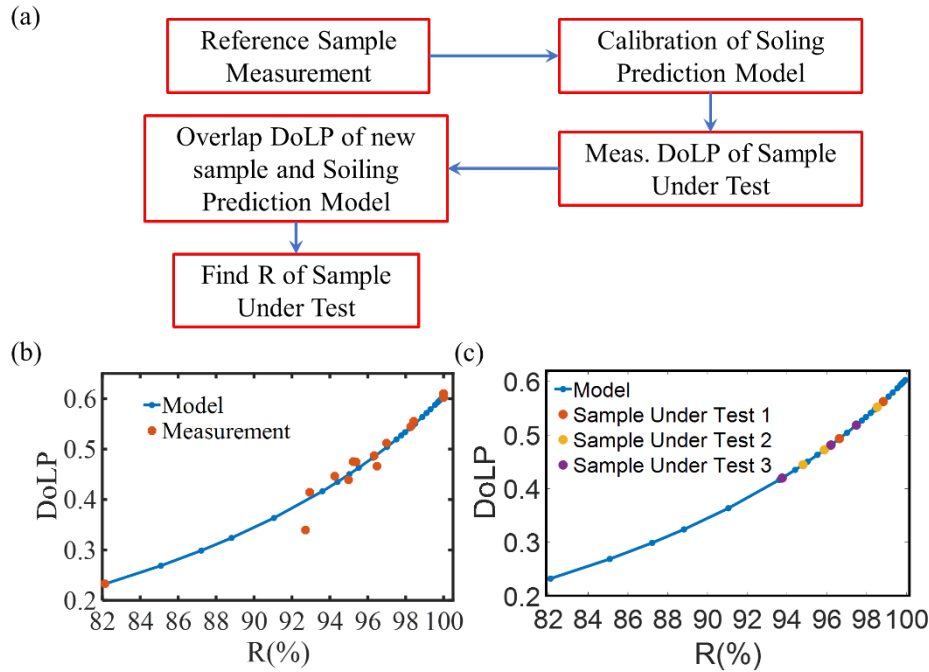


Figure 5. (a) Overall procedure of soiling prediction (b) model fitting results: the simulated and measured DoLP vs. relative reflection of reference soiled mirror (c) soiling level (relative reflection coefficients) determination of three samples based on the fitted model in Fig. 8b, the average DoLP of the soiled mirrors under test suggest the corresponding reflection coefficients based on the fitted model, i.e., the DoLP vs. reflection curve. The measurement and the simulation model are performed on a clear sunny day (03/01/2022) at 3:18pm. Location Arizona State University Church parking lot roof (33.419258°, -111.929590°). Camera location azimuth, $\Phi=330^\circ$ and zenith, $\theta=65^\circ$.

Now, to quantify the soiling levels of the samples in, Figure 4, we first measured the DoLP of some reference samples with known soiling levels and used the results to calibrate the soiling prediction model. Note that this is necessary for accurate measurement because the skylight polarization state is highly dependent on the weather condition and cloud coverage. Moreover, the skylight and sunlight ratio also varies, which also impacts the model. For the calibration, we utilized the same measurement setup as illustrated in Figure 1a. We position our camera toward the uniform and maximum DoLP region (around $\Phi=330^\circ$ and $\theta=65^\circ$, in Figure 3c) and take the image of the mirror. After taking the image, we process it to produce the DoLP image. From the DoLP image, we can determine the average DoLP values for different soiled sections and corresponding standard deviations for the best measurement accuracy and reliability. The relative reflection of each section of the reference sample was measured using an unpolarized white light source (visible wavelength range, divergence angle $\sim 10^\circ$) and a power meter (S302C-Thermal Power Sensor Head, Surface Absorber, 0.19 - 25 μm , 2 W, $\varnothing 12$ mm, Thorlabs Inc.) in the lab. For this measurement, we first measured the reflected light power from the clean part of the mirror. The reflected power from the clean part of the mirror is taken as a reference or baseline. Then we measured the reflected power from all the other sections of all mirror samples. The reflected powers from

all different sections are divided by the reflected power from the clean part to obtain the relative reflection of each section of the samples. So, if the clean mirror has less than 100% reflection, real reflection efficiencies of the soiled regions can be obtained by multiplying the relative reflection efficiencies with the reflection of the clean mirror. Reflection from each section of all the soiled samples is measured at least three times to increase the reliability of the measurement, calculate the mean value and determine the standard deviation. The DoLP vs. reflection, R, (or soiling level) of the known samples are used to calibrate the soiling level predicting model to account for different weather conditions and the ratio of skylight and sunlight ($R_{Sun} : R_{Sky}$) during the measurement. The whole process of soiling level prediction is described in the flow chart in Figure 5a. The DoLP vs. R curve for the reference samples and the fitted model is shown in Figure 5b.

After the calibration, the soiling prediction model provided the relation between DoLP and relative reflection, R. The soiling level of the unknown mirror samples was determined by obtaining the corresponding R with the measured DoLP images for each soiled mirror section in Figure 4d-f. The results are shown in Figure 5c. Considering the median value of the DoLP for each section of the soiled samples of SUTs, the predicted median soiling level of SUT1 is 98.84%, 96.19%, and 96.63%; for SUT2, they are 98.53%, 95.87%, 94.80% and for SUT3 they are 97.49%, 96.21%, 93.76%. Also, considering the DoLP range, presented in Figure 4d-f, the reflection efficiency range of each section for each sample is presented in Figure 6a-c (blue curve).

2.4 Measurement Accuracy Analysis

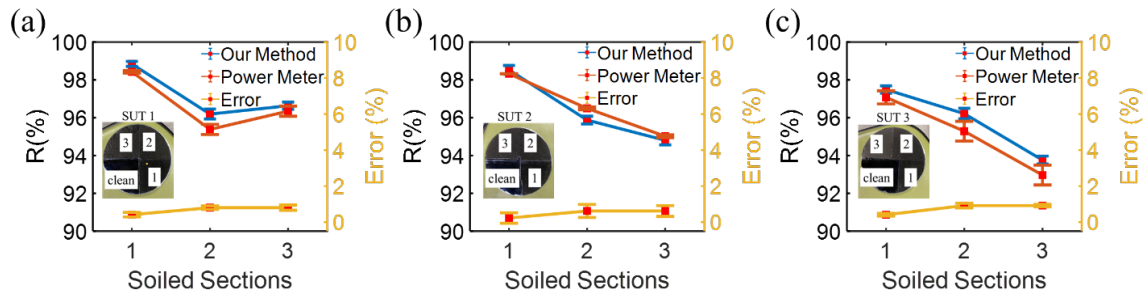


Figure 6. Soiling or relative reflection measured with our method and large area reflection measurement with a power meter and error for (a) sample under test 1 (SUT 1) (b) SUT 2 (c) SUT 3. The measurement and the simulation model are performed on a clear sunny day (03/01/2022) at 3:18pm. Location Arizona State University Church parking lot roof (33.419258°, -111.929590°). Camera location azimuth, $\Phi=330^\circ$ and zenith, $\theta=65^\circ$.

To evaluate the accuracy of the predicted relative reflection or soiling levels of the mirror samples, we performed the reflection measurement of the samples in the same way as described in the previous section. The relative reflection coefficients of all three samples obtained with the polarization imaging method and those obtained from reflection measurement are shown on the same plot for comparison in Figure 6. The measurement errors, also shown in Figure 9, between these two methods are less than 1% for all the samples. Such a level of accuracy makes it possible to use polarization images to identify different soiling levels on the heliostat mirrors. However, the high measurement accuracy relies on accurate calibration of the soiling level prediction model, which requires a carefully planned procedure for future CSP field deployment.

3. Conclusion

In conclusion, we have demonstrated a polarimetry-based mirror soiling level detection method in regular daylight conditions. It is field deployable and can be applied to monitor the soiling of the heliostat mirrors in the CSP plant to provide information for making cleaning schedules and soiling pattern studies. In the future, we plan to utilize a polarimetric imaging drone [12] to take pictures of the heliostat fields for quick evaluation of the soiling condition over large areas of mirrors. The proposed method can significantly reduce the measurement time compared with conventional methods with handheld reflectometers. Moreover, the method developed in this paper can also help us investigate the soiling pattern in different weather conditions and seasons to facilitate soiling forecasts for different seasons and environmental conditions.

Author contributions

Md Zubair Ebne Rafique contributed to sample preparation, developing the measurement procedure and setup, performing measurements, data post-processing, and analysis, developing the simulation model and soiling prediction methodology, writing the original draft, and reviewing and editing manuscript drafts.

Hossain Mansur Resalat Faruque contributed to sample preparation, developing the measurement setup, performing measurements, and data post-processing.

Ahmad Hassan contributed to developing the measurement setup, image processing, and performing measurements.

Mo Tian contributed to sample preparation and performing measurements.

Nabasinghu Das contributed to performing measurements.

Yu Yao contributed to conceptualization, experiment design, data analysis, supervision, project administration, and reviewing and editing manuscript drafts.

Competing interests

The authors declare no competing interests.

Funding

The research conducted at Arizona State University is supported by the U.S. Department of Energy Solar Energy Technology Office under the contract no. EE0008999. Sandia National Laboratories is a multi-mission laboratory managed and operated by National Technology & Engineering Solutions of Sandia, LLC, a wholly-owned subsidiary of Honeywell International Inc., for the U.S. Department of Energy's National Nuclear Security Administration under contract DE-NA0003525.

Reference

1. J. Coventry, C.-A. Asselineau, E. Salahat, M. A. Raman, and R. Mahony, "A robotic vision system for inspection of soiling at CSP plants," presented at the SOLARPACES 2019: International Conference on Concentrating Solar Power and Chemical Energy Systems, Daegu, South Korea, 2020, p. 100001. doi: 10.1063/5.0029493.

2. F. Wolfertstetter, K. Pottler, A. A. Merrouni, A. Mezrhab, and R. Pitz-Paal, "A Novel Method for Automatic Real-Time Monitoring of Mirror Soiling Rates," p. 9.
3. G. Picotti, M. Binotti, M. E. Cholette, P. Borghesani, G. Manzolini, and T. Steinberg, "Modelling the soiling of heliostats: Assessment of the optical efficiency and impact of cleaning operations," presented at the SOLARPACES 2018: International Conference on Concentrating Solar Power and Chemical Energy Systems, Casablanca, Morocco, 2019, p. 030043. doi: 10.1063/1.5117555.
4. F. Wolfertstetter, R. Fonk, C. Prah, M. Röger, S. Wilbert, and J. Fernández-Reche, "Airborne soiling measurements of entire solar fields with Qfly," presented at the SOLARPACES 2019: International Conference on Concentrating Solar Power and Chemical Energy Systems, Daegu, South Korea, 2020, p. 100008. doi: 10.1063/5.0028968.
5. S. Meyen, E. Lupfert, D. G. A. Center, and A. Fernandez-Garcia, "Standardization of Solar Mirror Reflectance Measurements - Round Robin Test: Preprint," p. 11.
6. R. Wang, P. Borghesani, M. E. Cholette, B. Duck, L. Ma, and T. A. Steinberg, "In-situ reflectivity monitoring of heliostats using calibration cameras," presented at the SOLARPACES 2018: International Conference on Concentrating Solar Power and Chemical Energy Systems, Casablanca, Morocco, 2019, p. 030062. doi: 10.1063/1.5117574.
7. G. G. Stokes, Ed., "On the Composition and Resolution of Streams of Polarized Light from different Sources," in *Mathematical and Physical Papers*, in Cambridge Library Collection - Mathematics, vol. 3. Cambridge: Cambridge University Press, 2009, pp. 233–258. doi: 10.1017/CBO9780511702266.010.
8. S. Chandrasekhar, *Radiative transfer*. Courier Corporation, 2013.
9. C. F. Bohren and D. R. Huffman, *Absorption and Scattering of Light by Small Particles*. John Wiley & Sons, 2008.
10. C. Matzler, "MATLAB functions for Mie scattering and absorption," *IAP Res Rep*, vol. 8, Jul. 2002.
11. M. Z. E. Rafique, "Nanophotonics for Ultrafast Optical Modulation, Ocean, and Energy Applications," Ph.D., Arizona State University, United States -- Arizona, 2022. Accessed: Jan. 13, 2023. [Online]. Available: <https://www.proquest.com/docview/2758586858/abstract/90083E9A6E6E4DC5PQ/1>
12. M. Tian et al., "Toward Autonomous Field Inspection of CSP Collectors with a Polarimetric Imaging Drone," *SolarPACES*, 2022.